ADVANCED HEALTHCARE MATERIALS
www.advhealthmat.de

Glioblastoma Spheroid Invasion through Soft, Brain-Like Matrices Depends on Hyaluronic Acid–CD44 Interactions

*Gevick Safarians, Alireza Sohrabi, Itay Solomon, Weikun Xiao, Soniya Bastola, Bushra W. Rajput, Mary Epperson, Isabella Rosenzweig, Kelly Tamura, Breahna Singer, Joyce Huang, Mollie J. Harrison, Talia Sanazzaro, Michael C. Condro, Harley I. Kornblum, and Stephanie K. Seidlits**

Increased secretion of hyaluronic acid (HA), a glycosaminoglycan abundant in the brain extracellular matrix (ECM), correlates with worse clinical outcomes for glioblastoma (GBM) patients. GBM cells aggressively invade the brain parenchyma while encountering spatiotemporal changes in their local ECM, including HA concentration. To investigate how varying HA concentrations affect GBM invasion, patient-derived GBM cells are cultured within a soft, 3D matrix in which HA concentration is precisely varied and cell migration observed. Data demonstrate that HA concentration can determine the invasive activity of patient-derived GBM cells in a biphasic and highly sensitive manner, where the absolute concentration of HA at which cell migration peaked is specific to each patient-derived line. Furthermore, evidence that this response relies on phosphorylated ezrin, which interacts with the intracellular domain of HA-engaged CD44 to effectively link the actin cytoskeleton to the local ECM is provided. Overall, this study highlights CD44–HA binding as a major mediator of GBM cell migration that acts independently of integrins and focal adhesion complexes and suggests that targeting HA–CD44–ezrin interactions represents a promising therapeutic strategy to prevent tumor cell invasion in the brain.

1. Introduction

Glioblastoma (GBM) is the most common, lethal, and aggressive form of primary central nervous system (CNS) cancer.[1,2] Even after surgical resection, radiotherapy, and adjuvant chemotherapy, long-term survival is rare. Among GBM patients receiving this conventional, aggressive treatment, median survival is 12–15 months and the 5-year survival rate is around 6%.[3,4] GBM tumors aggressively invade the brain parenchyma, with recurrent tumors appearing most often near the resection site of the primary tumor.[5] Extraneural GBM metastases are rare[6] and, instead, GBM cells preferentially migrate along defined structures in the brain, known as the secondary structures of Scherer.[6,7] Together, these observations suggest that mechanochemical features of brain microenvironment are uniquely conducive to GBM cell infiltration and invasion.

Brain tissue is enriched with high molecular weight forms of hyaluronic acid (HA), a linear-chain, unsulfated, glycosaminoglycan of repeating D-glucuronic acid and *N*-acetyl-D-glucosamine disaccharide subunits.[8] HA and other glycoproteins form the 3D extracellular matrix (ECM) through which GBM cells infiltrating the brain parenchyma must navigate. In GBM tumors, increasing expression of HA, HA synthases, and hyaluronidase correlates with disease progression.[9–12] To improve our understanding of how these changes may drive tumor invasion, effects of HA concentration on invasion of patient-derived GBM spheroids into 3D biomaterial scaffolds were investigated.

The relationship between cell–ECM adhesions and cell migration has been explained by the "motor-clutch" model of cell migration, where receptor–ECM adhesions act as "clutches" that determine traction forces exerted by myosin motors on polymerized actin to drive migration.[13,14] As predicted by the "motor-clutch" model, cells typically exhibit a classic biphasic relationship between migration speed and ECM concentration, where speed increases with increasing ECM availability up to a maximum, at which point migration speed decreases with increasing ECM.[15–18] While this phenomenon has been well

G. Safarians, A. Sohrabi, I. Solomon, W. Xiao, S. Bastola, B. W. Rajput, M. Epperson, I. Rosenzweig, K. Tamura, B. Singer, J. Huang, S. K. Seidlits
Department of Bioengineering
University of California Los Angeles
Los Angeles, CA 90095, USA
E-mail: seidlits@utexas.edu

A. Sohrabi, M. J. Harrison, T. Sanazzaro, S. K. Seidlits
Department of Biomedical Engineering
The University of Texas at Austin
Austin, TX 78712, USA

S. Bastola, M. C. Condro, H. I. Kornblum
Semel Institute for Neuroscience and Human Behavior
University of California Los Angeles
Los Angeles, CA 90024, USA

The ORCID identification number(s) for the author(s) of this article can be found under https://doi.org/10.1002/adhm.202203143

DOI: 10.1002/adhm.202203143

characterized for integrin–ECM interactions, independent effects of CD44–HA interactions in this model have remained largely unexplored.[15,19–25] The "motor-clutch" model of cell migration requires that matrix-engaged receptors be tethered intracellularly to the actin cytoskeleton, typically through adaptor proteins. For example, focal adhesions, comprised of integrins and adaptor proteins, dynamically rearrange to oppose the force exerted by their surrounding matrix, a process dictating a cell's ability to move.

A similar mechanism may present through CD44 via the ezrin adapter protein, which anchors the intracellular domain to actin filaments in its phosphorylated, "open" state.[26,27] In this tethered state, additional adapter proteins (e.g., radixin and moesin), transmembrane proteins (e.g., CD44, integrins, and tyrosine kinase receptors), and actin fibers are recruited to the sites of matrix-bound CD44.[27–29] The degree of recruitment depends on the number of bound CD44 receptors, extent of ezrin phosphorylation, and the physical force exerted by the ECM at the adhesion site.[27,29] These complexes are thought to act as "clutches" regulating migration speed based on adhesion forces.[25,30] In murine models, one study reported that intermediate levels of CD44 expression by xenografted GBM cells were observed in the most aggressive tumors, supporting the theory that CD44 acts as a molecular clutch.[19] However, in reality the role of CD44–HA interactions in cell migration are likely more complex. For example, CD44 can act as mechanosensor, mediating effects of substrate stiffness on cell proliferation and motility.[31] In addition, previous work by our group has found that GBM cells require both integrin and CD44 engagement for invasion through soft, 3D matrices.[32]

In addition to the "motor-clutch" model,[25,30] CD44 receptors during cell migration (and other activities requiring substantial cytoskeletal and membrane rearrangements) have also been described using the anchored "picket-fence" model.[33–35] In this model, actin fibers are considered the "fences" which are joined by CD44 "pickets" when actively tethered by ezrin. The "pickets" form barriers with the cell membrane creating localized "corrals" that confine diffusion other membrane-bound proteins, including integrins, from crossing the "fences."[35] Thus, with more "pickets," membrane diffusion and clustering of integrins and CD44 are reduced, effectively preventing a local increase membrane tension within the "corral." This mechanism is key for many cell activities requiring membrane polarization, including phagocytosis and chemotaxis.[35–37]

Like HA expression, ezrin activity and CD44–ezrin interactions have long been associated with aggression and metastasis in several cancers, including breast cancer[37,38] and osteosarcoma.[26,39–41] Both CD44 and ezrin mediate cancer cell proliferation and metastatic invasion through pathways well-known to drive disease progression and cell migration, including Akt/mTOR, Ras/Rac, and RhoA.[26,42] Past studies have demonstrated reduced growth of xenografted GBM tumors in mouse models and reduced proliferation in vitro with inhibition of either moesin or radixin activity.[43,44] However, effects of HA concentration, along with the mechanisms behind these effects, on tumor cell migration in three dimensions through very soft, low tension matrices resembling brain tissue, as experienced by invading GBM cells, have yet to be thoroughly investigated.

Biomaterial approaches to model the brain ECM in 3D cultures have been previously developed to investigate the effects on ECM parameters on the invasive capacity through a 3D matrix. In general, these studies have reported that HA concentration, matrix stiffness, concentration of integrin-binding sites, and scaffold porosity each affect GBM cell migration. However, previous fabrication methods for 3D culture scaffolds did not adequately decouple these features and/or vary the HA concentration, making it difficult to discern the independent effects of HA concentration.[45–50] While wide ranges of stiffnesses for brain and GBM tumors have been reported,[51] this study focused on very soft biomaterials representing the lower end of this range based on our previous findings that when patient-derived GBM cells are cultured in very soft 3D scaffolds (≈100 Pa shear storage modulus or 1 kPa Young's modulus) it exhibited behaviors, such as treatment resistance, that more closely resembled in vivo behaviors, compared to culture in marginally stiffer scaffolds (≈250 Pa shear storage modulus; 2.5 kPa Young's modulus).[52] Furthermore, when incorporating HA into 3D scaffolds, both the molecular weight and degree of chemical modification of HA have profound effects on bioactivity, including activation of the CD44 receptor.[53,54] Here, we used a HA with high molecular weight (nominal 700 kDa), to best represent HA in the native brain ECM,[55] that was minimally modified, where a thiol group was added to ≈5% of disaccharides.[52] In addition, we sought to investigate the effects of HA concentration over a range (0.1–0.75% w/v) that encompasses the range of physiological HA concentrations[56–58] present in normal brain. However, many previous studies used scaffold fabrication methods that required both high degrees of HA modification (e.g., >50%) and a minimum of 1% w/v HA in biomaterial scaffolds.[47–50] To achieve a lower concentration range of unmodified, high molecular weight HA in a 3D scaffold, researchers have physically embedded soluble HA into a collagen fiber network.[46,59] However, altering the concentration can alter the fiber size in the network, which in and of itself may affect cell migration.[60] Together, insufficient decoupling of migratory cues may be responsible for inconsistent results across these previous studies.

Here, we fabricated 3D culture matrices in which HA concentration could be varied from 0.10–0.75% weight per volume (w/v) while maintaining constant, brain-mimetic mechanical properties, availability of integrin-binding RGD sites, and solute permeability. This culture platform enabled a systematic investigation of the effects of HA concentration on the invasion of encapsulated, patient-derived GBM spheroids which are genotypically and phenotypically different from and more clinically representative than transformed GBM cell lines (e.g., U87-MG) used in many previous studies.[47,49,59,61] Across this physiologically relevant range of HA concentrations, results show that GBM cell migration in a 3D matrix is closely linked to HA concentration and CD44–ezrin–actin anchoring, with cells derived from specific patient tumors showing clear biphasic responses.

2. Results

2.1. Higher Grade Gliomas Secrete Greater Levels of HA

Like many solid tumors, GBM tumors oversecrete HA.[62–64] To assess potential differences in HA deposition in clinical brain

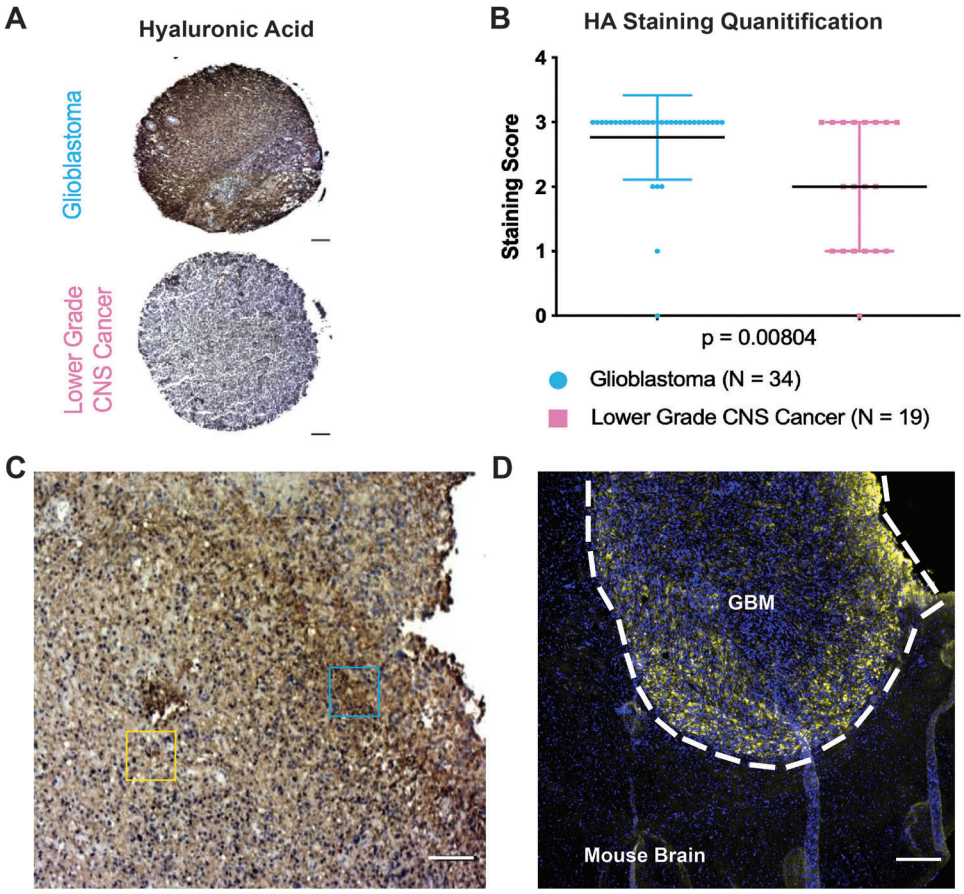

Figure 1. HA deposition increases in CNS tumors, including GBM. A) Representative image of immunohistochemistry of patient tissue microarrays (TMAs). Brown, positive HA stain; dark blue, hematoxylin. Scale bar = 100 µm. B) Categorical scoring of 34 GBM and 19 lower-grade CNS cancer tissues. Mann–Whitney U Test statistical test was used. C) Expanded image of patient-resected GBM tissue. Blue square = area of high HA concentration. Yellow square = area of low HA concentration. Scale bar = 100 µm. D) HA (yellow) staining images of HK408 xenograft. Nuclei (Hoechst 33324) shown in blue. Scale bar = 200 µm.

tumors, we immunostained tissue microarray (TMA) samples, provided without any identifying information by the UCLA Brain Tumor Tissue Resource, for HA in GBM (N = 34) and lower-grade CNS (N = 19) sections of tumors resected from patients. Representative images of tissue samples are shown in **Figure 1**A. Quantification showed elevated HA concentration in GBM tissues, also known as grade IV glioma, relative to lower grade CNS cancers (Figure 1B). The spatial distribution of HA in patient tissues was nonuniform, containing regions with relatively higher (darker brown) and lower (lighter brown) HA concentrations (Figure 1C). Following orthotopic implantation in mice, HK408 cells also exhibited greater HA deposition, especially along the tumor edge where invasion into the parenchyma occurs (Figure 1D).

2.2. Fabrication of 3D Culture Matrices with Tunable HA Concentration

To investigate the effects of different HA concentration on GBM cell phenotypes, we encapsulated gliomaspheres (GSs) in mechanochemically tunable, 3D hydrogels, as previously described by Liang et al. (2022).[65] Specifically, we fabricated HA hydrogels with 0.10%, 0.25%, 0.50%, or 0.75% weight per volume (w/v) HA. Concentrations were chosen to approximate physiological ranges of HA in mammalian CNS tissues.[56,57] To control extraneous variables affecting cell phenotypes, we ensured spheroid-laden hydrogels across experiments contained 0.025% w/v RGD peptides, were exposed to equal UV doses during gelation, and had comparable mechanical properties. Hydrogels had comparable storage (G', 0.10% HA = 115.1 ± 14.2 Pa, 0.25% HA = 116.3 ± 19.0 Pa, 0.5% HA = 116.3 ± 20.3 Pa, 0.75% HA = 124.4 ± 16.3 Pa) and loss (G'', 0.10% HA = 2.9 ± 0.9 Pa, 0.25% HA = 4.8 ± 0.9 Pa, 0.5% HA = 3.7 ± 0.6 Pa, 0.75% HA = 4.9 ± 0.7 Pa (**Figure 2**A and Figure S1A, Supporting Information). Similar storage and loss moduli were observed across the hydrogel conditions, confirming that differences in viscoelasticity were not responsible for observed differences (Figure S1A, Supporting Information). Storage moduli in the range of 100–150 Pa approximate those for healthy brain tissue.[66,67] Swelling characterization was performed by incubating priorly weighed hydrogels in Dulbecco's phosphate buffered saline (D-PBS) for 24 h. The ratio of the final to initial mass, or mass swelling ratio, gradually increased with increasing

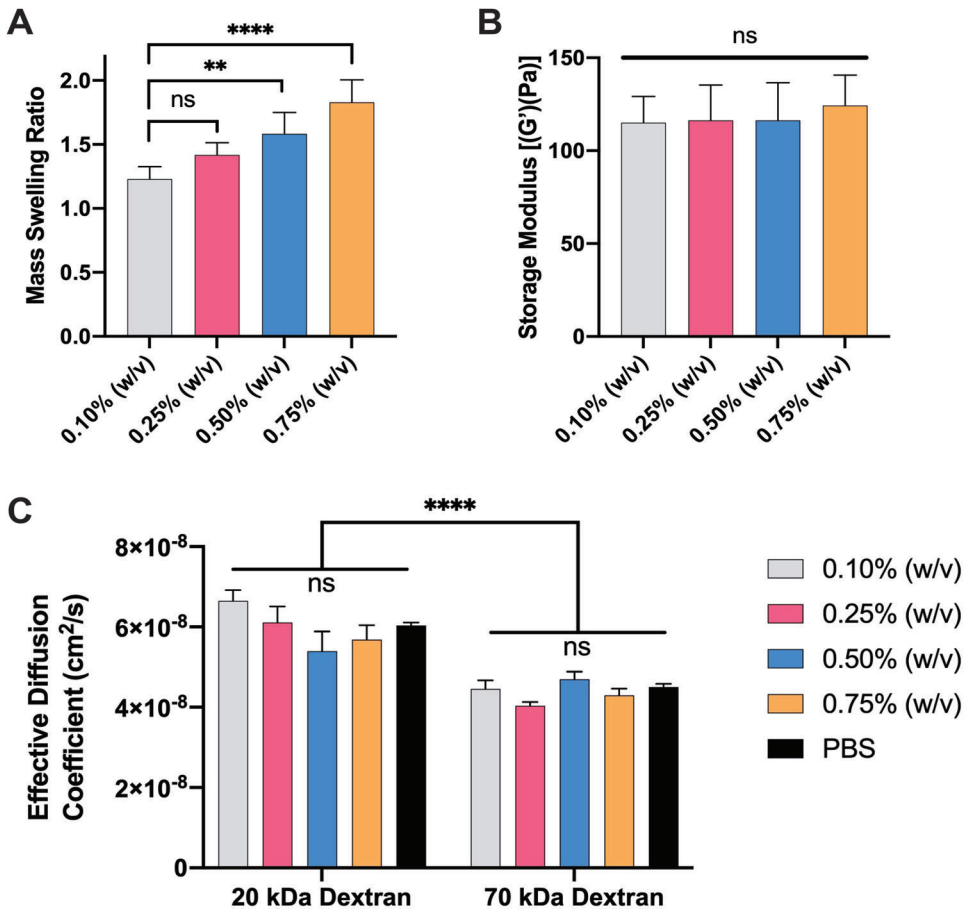

Figure 2. Characterization of hydrogel matrices for 3D cell culture. A) Mass swelling ratios of individual hydrogels following fabrication. One-way ANOVA statistical test was used follwed by post-hoc Tukey's multiple comparisons test of significance. B) Storage moduli (G') of hydrogels with varying HA concentrations. One-way ANOVA statistical test was used followed by Tukey's post-hoc test of significance. C) Effective diffusion coefficients, as measured using FRAP, of 20 and 70 kDa FITC–dextran polymers through hydrogels with varying HA concentrations or D-PBS buffer. Two-way ANOVA statistical test was used followed by Tukey's post-hoc test of significance. *, $p < 0.05$; **, $p < 0.01$; ***, $p < 0.001$; ****, $p < 0.0001$.

HA concentrations in hydrogels (Figure 2B). This result is not unexpected, given the hygroscopic properties of HA.[68,69] While differences in water content may have effects on cell interactions with hydrogel matrices, solute diffusion through 3D hydrogel matrices remained similar. Using fluorescence recovery after photobleaching (FRAP), we found the effective diffusion rates of 20 and 70 kDa fluorescein isothiocyanate-dextran (FITC–Dextran) solutes in all hydrogel conditions were equivalent to dextran diffusion through D-PBS solutions (Figure 2C). These results confirmed that solutes of 70 kDa or lower, including the growth factors and small molecule inhibitors used in these experiments, could freely diffuse through hydrogels.

To allow for cell–cell adhesions and paracrine interactions among tumor cells, as would normally be present within brain tumors, GSs ≈150 µm in diameter were encapsulated within 3D hydrogels for culture. Experiments were performed across four unique GBM cell lines, derived from individual patients, designated here as HK408, HK177, HK217, and GS054. Full analysis of molecular alterations, through genomic and transcriptomic sequencing, were performed by the labs of Dr. Harley Kornblum (HK408, HK177, and HK217) and Dr. David Nathanson (GS054) at UCLA at the time of sample collection. Based on the subtype classifications specific by Verhaak, et al. (2010),[70] HK408 and HK217 were classified as proneural and HK177 as mesenchymal.[71] GS054 was classified as a mix of both classical and mesenchymal subtypes, given mutations in PTEN, NF1, and CDKN2A genes.[70]

Quantification of a live/dead assay confirmed that GSs from patient-derived GBM cell lines remained viable over the 6-day experimental period, regardless of the HA concentration in the hydrogel matrix (**Figure 3**A). In general, viability of HK408 GSs was above 75% 24 h following 3D encapsulation in all hydrogel formulations (Figure S1B, Supporting Information). Apoptosis was assessed via immunostaining for cleaved-PARP (Cl-PARP). Less than 10% of cells in GSs were apoptotic across 3D culture conditions (Figure 3B). Specifically, after 24 h in 3D culture, HK408 GSs in 0.10%, 0.25%, 0.5%, and 0.75% w/v HA hydrogels had 6 ± 2%, 3 ± 2%, 3 ± 1%, and 3 ± 1% apoptotic cells, respectively, while GS054 GSs had 2 ± 1%, 2 ± 1%, 2 ± 1%, and 2 ± 1% apoptotic cells, respectively. A significantly greater apoptotic percentage was evident for HK408 cells in 0.10% w/v HA cultures, as compared to those with higher HA content. This is not

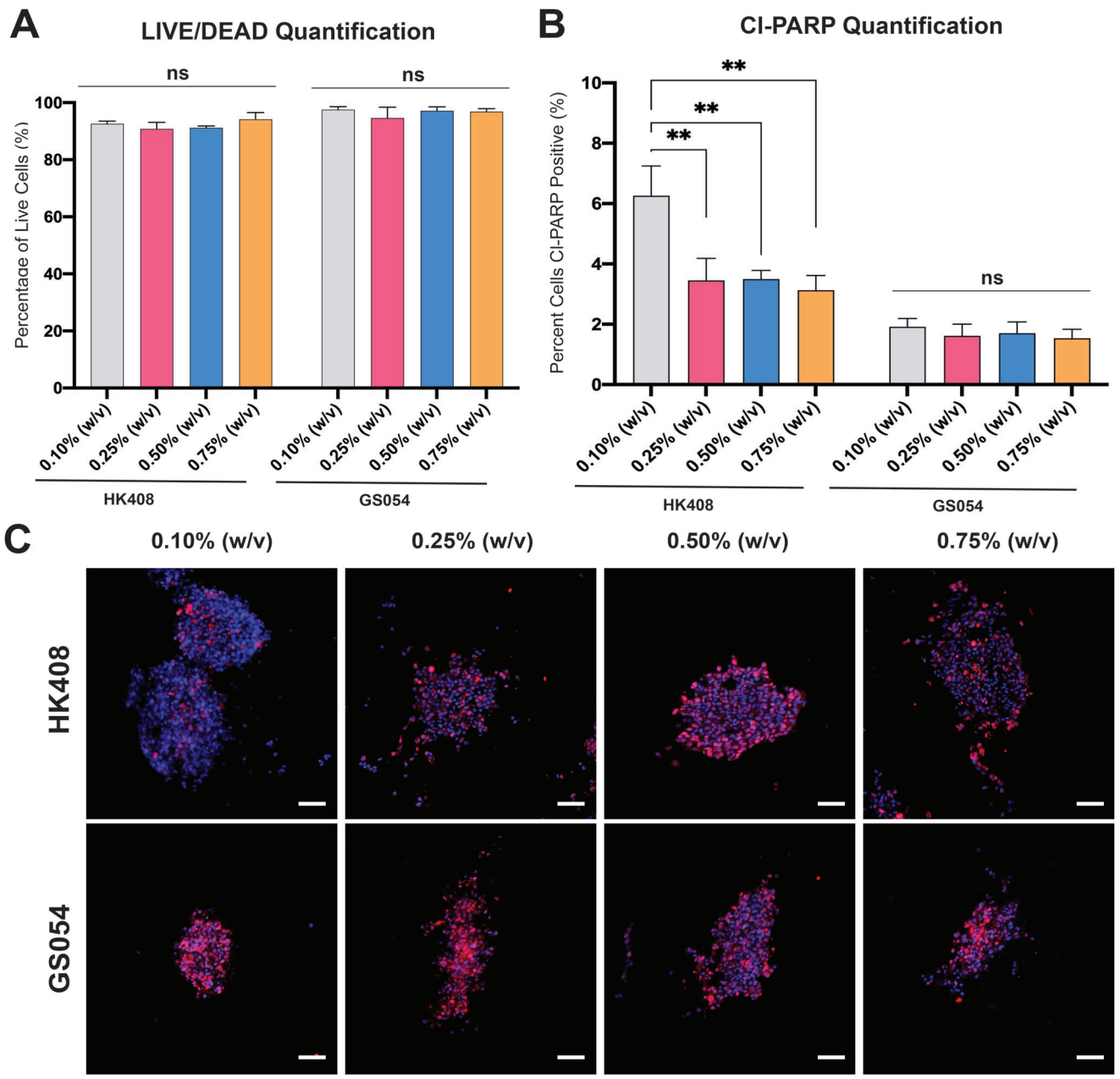

Figure 3. Characterization of GS viability in 3D culture matrices. A) LIVE/DEAD stain quantification was performed to assess cell viability following 6 days in culture for HK408 and GS054 GSs. B) Quantification of Cl-PARP positive cells in HK408 and GS054 GS sections following 6 days in culture. For all data, one-way ANOVA statistical test was used followed by post-hoc Tukey's multiple comparisons test of significance for each patient line. C) Representative images of Ki67 staining of HK408 and GS054 GS cryosections following 6 days in culture. Red = Ki67; Blue = Hoechst 33342. Scale bars = 50 µm. **, $p < 0.01$; ***, $p < 0.001$; ****, $p < 0.0001$.

unexpected, as previous reports have found that HA can increase GBM cell survival.[19,32,72] Additionally, we performed immunostaining for the proliferation marker Ki67, which we found was heavily expressed by most cells within GSs across hydrogel conditions (Figure 3C). The exceptional group was the HK408 GSs in 0.10% w/v HA hydrogel. In line with viability data, HK408 GSs in 0.10% w/v HA had observably fewer proliferative cells (Ki67+) than those in 0.25%, 0.50%, or 0.75% w/v HA hydrogels. This observation was further confirmed for HK408 cells using an EdU assay for proliferation (Figures S1C and S2, Supporting Information).

2.3. Relationships between HA Concentration and GS Invasion in Soft Matrices

Cell invasion from periphery of GSs' into the surrounding hydrogel matrix was clear by 24 h in 3D culture (Figure S3, Supporting

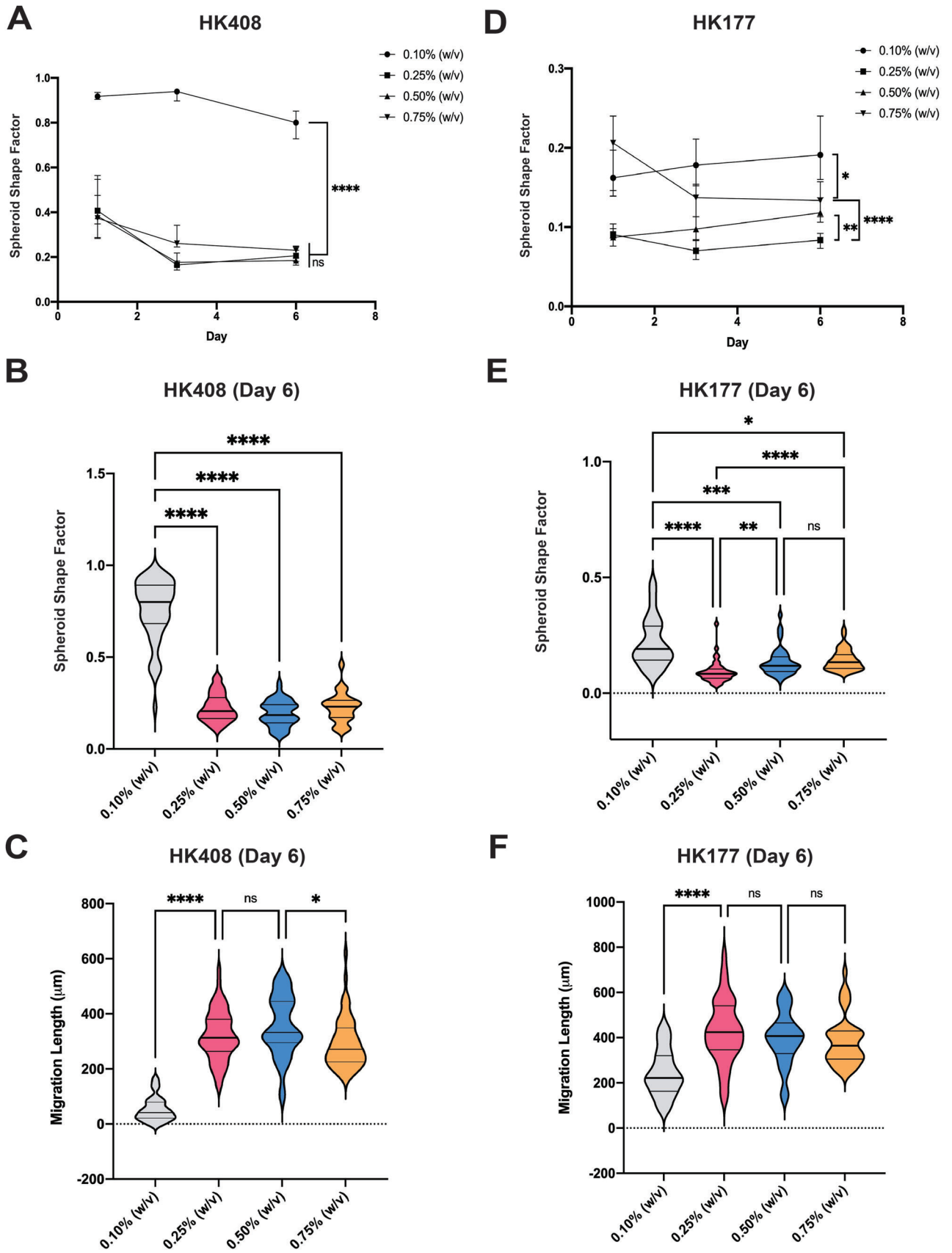

Information). GSs in 3D culture displayed diverse morphologies dependent on both HA concentration and the patient line. However, these morphologies were independent of the sub-type classification (proneural—HK408 and HK217 or mesenchymal—GS054 and HK177) assigned to the original patient tumor.[70] While HK408 and HK177 GSs displayed thicker, multicellular protrusions indicative of collective migration, HK217 and GS054 GSs displayed thinner, single cell protrusions extending into matrix (Figure S4A,B, Supporting Information). Still, individual instances of single and collective cell migration could be found in all patient lines. Uniquely, GS054 spheroids encapsulated in 0.75% w/v HA hydrogels adopted polarized, crescent-like shapes, which did not resemble the invasive phenotypes observed for GS054 in 0.10–0.50% w/v HA hydrogel cultures or for other cell lines (Figure S4B, Supporting Information).

Invasion of cells from 3D cultured GSs into hydrogel scaffolds was quantified over the course of 6 days for HK408, HK177, and GS054 cells. In comparison, invasion was slower from HK217 GSs and so migratory activity was assessed over 9 days. Invasion was quantified through two separate measurements, spheroid shape factor and migration length (Figure S5, Supporting Information). Spheroid shape factor represents the deviation from circularity of an individual GS over time as cell migrates out from the sphere periphery and provides a measure of overall invasive activity. The spheroid shape factor immediately after GS encapsulation is set as 1, while deviations from circularity, caused by GBM cell invasion into the matrix, are less than 1. Thus, a decreasing spheroid shape factor indicates increasing invasive activity. In contrast, migration length represents the maximum Euclidian displacement by a single cell or multicellular protrusion from the GS periphery into the matrix. Thus, an increasing migration length indicates that cells are able to invade further into the matrix, and away from the original GS. In general, GSs across patient lines were the least invasive in hydrogels with 0.10% w/v HA, with statistically significant differences in spheroid shape factor and migration length when compared to GSs in 0.25% w/v HA hydrogels (**Figures 4**A–F and **5**A–F and Figure S4A,B, Supporting Information).

GSs of HK408 and HK177 patient lines exhibited peak invasive activity around 0.25–0.50% w/v HA hydrogels, indicative of a classic biphasic relationship[15–18] between HA concentration and invasion, where invasion initially increases with increasing HA concentration until reaching a maximum in the first phase, then decreases with increasing HA concentration in the second phase (Figure 4A–F). For HK408 cells, differences in spheroid shape factor were non-significant for hydrogels with at least 0.25% w/v HA (Figure 4A,B). However, the median migration length of GSs in 0.75% w/v HA hydrogels was significantly less than for those in 0.50% w/v HA, indicating peak migratory activity in 0.25–0.50% HA hydrogels (Figure 4C). For HK177 GSs, the median spheroid shape factor for HK177 GSs was lower in hydrogels with 0.25% w/v HA than those with 0.50% or 0.75% w/v HA hydrogels, demonstrating peak migratory activity in 0.25% w/v HA cultures (Figure 4D,E). However, differences in migration lengths for HK177 GSs were only significant between 0.10% and 0.25% w/v HA cultures (Figure 4F).

Unlike for HK408 and HK177 cells, there was no HA concentration at which there was an obvious peak in migratory activity for GS054 and HK217 patient line. For spheroid shape factor and migration length measurements, GS054 GSs were most migratory in 0.75% w/v HA hydrogels, with no significant differences between the 0.25% and 0.50% w/v HA conditions (Figure 5A–C). While GS054 cell invasion increases with increasing HA concentration, this relationship is not linear and, qualitatively, appears to be reaching a plateau. In contrast, HK217 cell invasion increased substantially when the HA concentration increased from 0.10% to 0.25% w/v, but then experiences a plateau with a constant level of invasiveness, according to either spheroid shape factor or migration length measurements, across 0.25%, 0.50%, and 0.75% w/v HA (Figure 5D–F). As the GS054 and HK217 patient lines do not follow the classic biphasic relationship between ECM concentration and migratory activity,[16] these were denoted as "non-biphasic" (Figure S4B, Supporting Information).

2.4. Biphasic Response to HA Concentration Corresponds to Spatial Overlap of CD44 and Ezrin

Immunofluorescent staining for CD44 and ezrin (total protein, non-specific to phosphorylation state) was used to evaluate the relationships between HA concentration, CD44 recruitment of ezrin, and GS invasive capacity. In general, HK408 GSs, which exhibited a classic biphasic relationship between migratory activity and HA concentration, had high membrane expression of CD44, while GS054 GSs had sporadic CD44 expression (**Figure 6**A,B). There were no obvious differences in the intensities of CD44 signal from immunostaining across HA conditions for either HK408 or GS054 GSs. However, intensity of ezrin immunofluorescence was observably lower in for HK408 GSs cultured in 0.10% w/v HA hydrogels as compared to those cultured in 0.25–0.75% w/v HA hydrogels (Figure 6A).

There were clear differences in CD44 and ezrin colocalization at cell membranes in HK408 cells across HA concentrations. However, there was significantly less overlap of CD44 and ezrin immunostaining in hydrogel cultures with 0.10% w/v HA hydrogels than those with 0.25%, 0.50%, or 0.75% w/v HA (Figure 6C). Notably, these changes in membrane localization of CD44 and ezrin was not limited to cells in direct contact with the HA matrix at GS edges, but included cells located within the spheroid mass suggesting that HA content may affect cells not in direct contact with the hydrogel matrix (Figure 6A). Unlike HK408 GSs, GS054 GSs did not display a biphasic relationship between migratory activity and HA concentration within the range of HA concentrations explored here. Across varying HA concentrations, no differences in CD44–ezrin colocalization were apparent for GS054 GSs (Figure 6B,D).

Figure 4. Patient-derived GBM cells exhibiting classic biphasic relationships between HA concentration and invasion. A) Spheroid shape factor quantification of HK408 GSs from days 1 to 6. B) Spheroid shape factors of HK408 GSs at the end of 6th day in culture. C) Migration lengths of HK408 GSs at the end of 6th day in culture. D) Spheroid shape factor quantification of HK177 GSs from days 1 to 6. E) Spheroid shape factors of HK177 GSs at the end of 6th day in culture. F) Migration lengths of HK177 GSs at the end of 6th day in culture. For all data, Kruskal–Wallis statistical test was used followed by Dunn's multiple comparisons test of significance. *$p < 0.05$; **$p < 0.01$; ***$p < 0.001$; ****$p < 0.0001$.

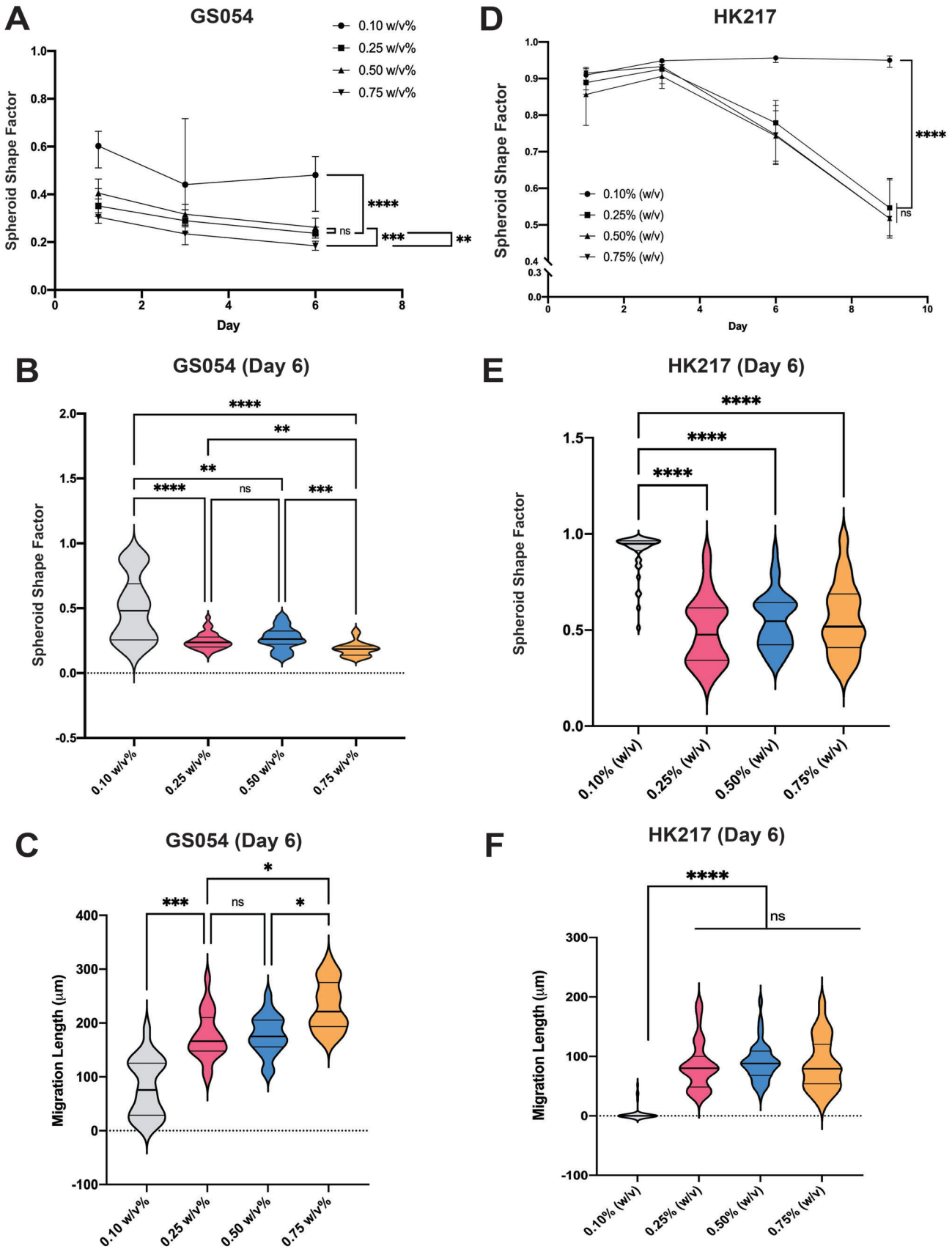

2.5. Effects of HA Concentration on Invasive Capacity Depend on Ezrin Phosphorylation

Constitutive knock-down of either CD44 or ezrin compromises cell proliferation, survival, and the ability of GSs to form.[52,73,74] Moreover, there is no well-established small molecule inhibitor targeting CD44 phosphorylation or CD44–ezrin binding. Thus, migration experiments were repeated with varying doses of a previously well-characterized, small-molecule inhibitor of ezrin phosphorylation, NSC668394,[39–41] to explore the mechanism of HA effects. For HK408 cells cultured in matrices with HA concentrations supporting migration (0.25%, 0.50%, and 0.75% w/v), 20 μM of NSC668394 successfully reduced migratory activity while lower concentrations had no significant effects (**Figure 7**A). At these HA concentrations, ezrin inhibition effectively disrupted extension of processes and invasive cell fronts from GSs and, thus, maximum migration length could not be calculated. However, migration of single, round cells from HK408 GSs clearly remained (Figure S6, Supporting Information). Notably, when cultured in matrices with only 0.10% w/v HA, treatment with NSC668394 increased HK408 cell migration (Figure 7A). With 5 μM NSC668394, small processes and single, rounded cells extended into the 0.10% w/v HA matrix. However, with 20 μM NSC668394, only single cells were observed, and cultures appeared very similar in all HA conditions (Figure S6, Supporting Information).

It is possible that untethering CD44 "pickets" from the actomyosin cortex, through NSC668394-mediated ezrin inhibition, may cause a larger relative reduction of membrane tension in matrices with a limited initial capacity for HA–CD44 engagement (i.e., 0.10% w/v HA compared to higher HA content) to support a more amoeboid-like migration.[22,59,75] This finding supports the popular hypothesis that the actin cortex must be sufficiently detached from both the cell membrane and the matrix for a cell to deform and migrate through a porous scaffold.[76] In matrices with sufficient HA-bound CD44 (i.e., 0.25–0.75% w/v HA) initially, treatment with NSC668394 uncouples CD44 from the actomyosin cortex but does not remove the CD44 tethering to HA in the ECM leaving one "fence" attached to the CD44 "picket."[76] Thus, the cells are not able to detach their membranes from the substrate and migrate using an amoeboid-type mode.[77,78] Additionally, when sufficiently decoupled from the actin cortex, ECM-bound CD44 "pickets" likely still inhibit membrane diffusion of integrins, reducing their ability to rearrange and generate traction forces needed for migration.

As discussed above, HK217 GSs were as sensitive to HA concentration as HK408 GSs, with higher rates of invasion in hydrogels with at least 0.25% w/v HA and little-to-no migration in those with 0.10% w/v HA. Like HK408 GSs, treatment with 5 μM NSC668394 increased migration of single, rounded cells in 0.10% w/v HA matrices (Figure 7B and Figure S6, Supporting Information). However, increasing NSC668394 dose to 10 or 20 μM effectively halted all cell migration, indicating that cells could not generate sufficient traction forces (Figure 7B and Figure S6, Supporting Information). For HK217 GSs in either 0.25% or 0.50% w/v HA hydrogels, GS invasiveness was inhibited by NSC668394 in a dose-responsive manner, with many cells appearing to die at the 20 μM dose. For HK217 GSs in 0.75% w/v HA matrices, 5 μM NSC668394 had no clear effects and 10 μM NSC668394 was required to inhibit invasion. This finding may be explained if the higher HA content results in increased numbers of HA–CD44 complexes and a downstream increase in ezrin phosphorylation, requiring more NSC668394 to achieve functional inhibition. Finally, for GS054 GSs the addition of NSC668394 at any concentration effectively inhibited invasion (Figure 7C and Figure S7, Supporting Information).

3. Discussion

This study sought to investigate the association between increased malignancy and expression of peritumoral HA and the CD44 receptor, which has been identified in cancers.[52,79–81] To better understand how HA–CD44 interactions influence invasiveness of GBM tumors, which reside in very soft, HA-rich brain tissue, we cultured spheroids of patient-derived GBM cells within 3D, bioengineered matrices in which HA concentration was varied. Results show that information about the local HA concentration is relayed through CD44–ezrin, with direct effects on GS invasiveness. Furthermore, relatively small variations in HA concentration were sufficient to significantly affect cell outgrowth from GBM patient-derived spheroids embedded and cultured within 3D matrices.

Hydrogel matrices for 3D cell culture were constructed using thiol-ene, photo-click chemistry which quickly forms stable covalent bonds under physiological conditions in the presence of live cells[65,82,83] relative to Michael addition reactions conventionally used to formulate HA hydrogels.[49,84–87] First, we thiolated high molecular weight HA, modifying ≈5% of its glucuronic acid groups,[88] which enabled a thiol-ene reaction with norbornene, provided here in the form of an 8-arm PEG.[65] At this degree of modification of HA chains with an average molecular weight of 700 kDa, we can estimate that on average the molecular weight between cross-link sites is ≈5 kDa. Thus, we incorporated branched PEGs into our hydrogel formulations with each branch being 5 kDa. We posit that inclusion of PEGs contribute to the lack of differences in hydrogel porosity, permeability, and stiffness across hydrogel conditions. Thiolated, 4-arm PEGs were introduced to reduce the HA concentration while maintaining a constant total polymer content. Increasing hydrogel swelling with increasing HA concentrations confirmed variations of HA between the different hydrogel formulations. Despite differences in swelling, hydrogel matrices had comparable porosity, permeability, and shear modulus across the range of HA concentrations investigated.

Figure 5. Patient-derived GBM cells that increase invasion with increasing HA concentration, but without a classic biphasic response. A) Spheroid shape factor quantification of GS054 GSs from days 1 to 6. B) Spheroid shape factors of GS054 GSs at the end of 6th day in culture. C) Migration lengths of GS054 GSs at the end of 6th day in culture. D) Spheroid shape factor quantification of HK217 GSs from days 1 to 6. E) Spheroid shape factors of HK217 GSs at the end of 6th day in culture. E) Spheroid shape factors of HK217 GSs at the end of 6th day in culture. F) Migration lengths of HK217 GSs at the end of 6th day in culture. For all data, Kruskal–Wallis ANOVA statistical test was used followed by post-hoc Dunn's multiple comparisons test of significance. *$p < 0.05$; ** $p < 0.001$; ***$p < 0.001$; ****$p < 0.0001$.

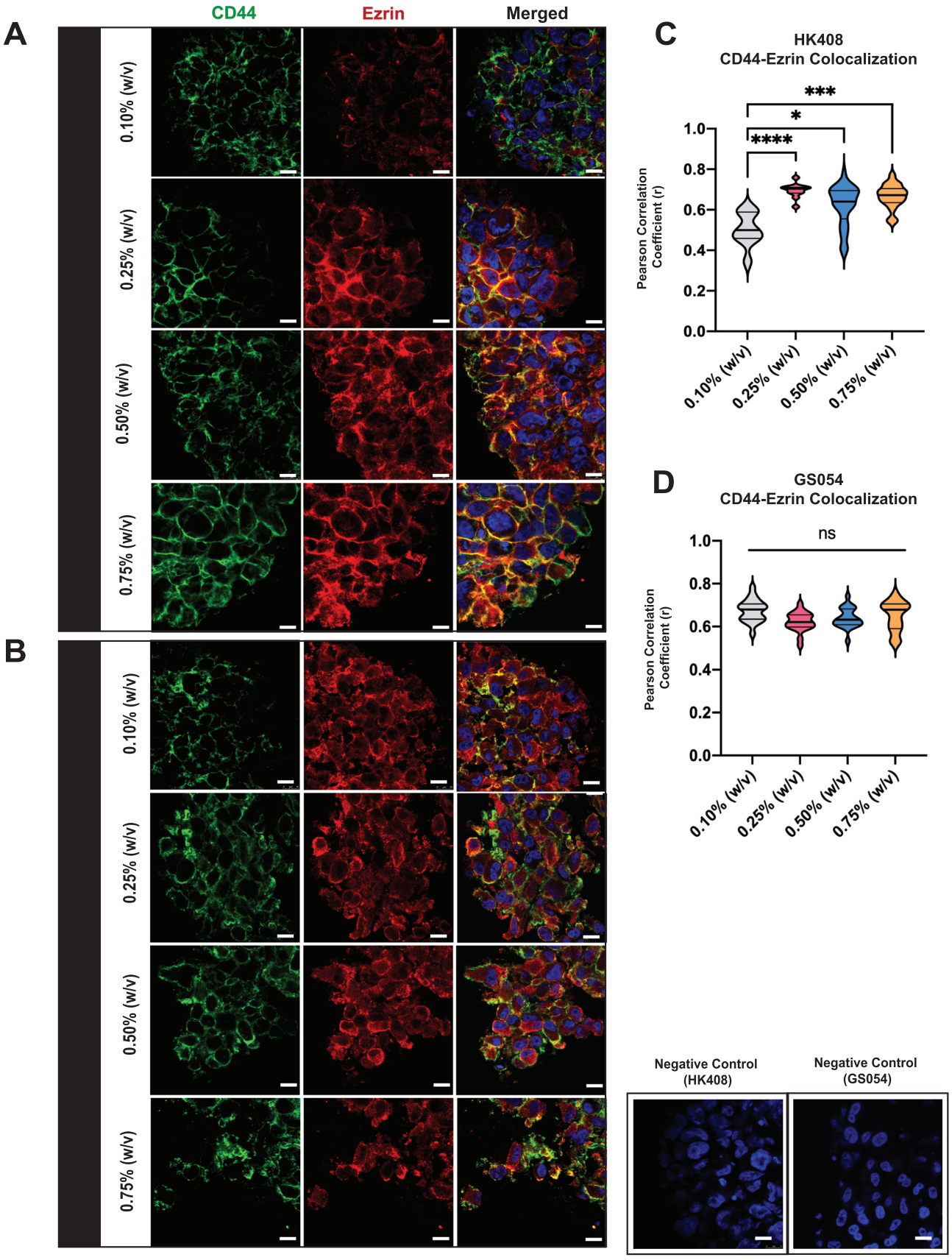

Thus, this approach was used to fabricate hydrogel matrices in which the effects of HA concentration on cell migration could be effectively decoupled from the effects of bulk mechanical properties and diffusive permeability. Furthermore, matrices were uniquely formulated to approximate several bioactive features of the brain ECM, including: 1) HA concentration varying across a single order-of-magnitude range and representing physiological HA ranges found in brain tissues,[56,57] and 2) low storage modulus (100–150 Pa) representing that of peritumoral brain tissue.[66,67] In addition, this study identified trends common to GBM cells derived from several individual patient tumors, rather than transformed GBM cell lines which often do not behave like patient-derived cells.[89,90] Overall, we anticipate this experimental design increases the physiological relevance of reported results.

Here, results indicate that HA concentration has biphasic effects on migratory activity and that CD44 receptors, like integrins, act as biochemical "clutches" (i.e., following "motor-clutch" theory of migration), where there exists a level of HA-bound CD44 with an adhesive force at which cell migration is maximized.[19,91] This finding is congruent with previous reports, which identified that expression of either too little or too much CD44 reduced the propensity for GBM cell invasion, implying an optimal "medium" expression level exists.[19,84,92] We then demonstrated how ezrin mediates 3D invasion of GBM cells by linking the intracellular domain of HA-bound CD44 to the actin cytoskeleton through ezrin. By physically tethering extracellular HA to the actin cortex, CD44–ezrin complexes have been theorized to act as "pickets" linking the HA and actin filament "fences" to control local membrane tension and diffusion of membrane-bound proteins.[33–35] However, further investigations into the mechanisms by which CD44 and ezrin regulate cell migration are warranted. Some studies have reported that CD44 and phosphorylated ezrin are concentrated at the leading edges of cells cultured on a hard, plastic surface, implying that CD44–ezrin increases migration by promoting local force generation.[37,93–95] Conversely, other studies have reported that CD44–ezrin interactions are sequestered toward the trailing edge of migrating cells, where they may act as "pickets" to inhibit nanoscale clustering of integrins and facilitating ECM detachment and increasing migration speed.[28,29,35,96,97] These seemingly conflicting findings of the roles of CD44 and ezrin may be attributed to experimental differences across previous studies. The stiffness of the substrate or matrix, availability of ECM-derived binding sites, and cell lines investigated likely all affect how cells migrate. For example, cell migration on very stiff, flat substrates likely requires alternative modes of force generation than migration through very soft, 3D matrices.

Here, we have demonstrated how HA concentration affects 3D cell invasion through CD44 and ezrin interactions. While previous work has relied primarily on CD44 engagement through uncontrolled, endogenously produced HA in the glycocalyx, in this study an exogenous HA matrix with 3D geometry was provided. Recently, local inhibition of CD44–ezrin interactions has been described as crucial to phagocytosis, a process which, like migration, involves dramatic restructuring of the cell membrane.[35,98] Specifically, CD44–ezrin "pickets" must detach from the actin filament "fences" to reduce tethering of the actin cortex to the cell membrane, effectively relieving membrane tension to allow for deformation. A similar process of membrane deformation must occur in amoeboid-type cell migration, where the cell membrane at the leading edge of the cell must deform to protrude into gaps within the 3D ECM and then propel its cytoplasmic contents forward before detaching and retracting the trailing edge.[76] Intravital imaging studies have suggested that invading cancer cells may predominately use amoeboid migration in vivo, where the ECM is generally softer than traditional culture substrates and cells can migrate within a 3D space.[38,99] In this study, when the ability of CD44–ezrin to bridge together the HA matrix and cytoskeleton was inhibited by low HA concentration in the 0.10% w/v matrix and with NSC668394, cells adopted an amoeboid-like migration mode in which adhesion to the matrix would be very low and likely inhibited by activation of the HA–CD44–ezrin axis. These results align with those from previous studies suggesting that very low adhesion and confinement (e.g., in matrix pores) is ideal for a transition from mesenchymal-to-amoeboid-like migration.[100–102]

HA concentration also had effects on viability of GBM cells, where cells cultured in matrices with low HA (0.10% w/v) had low viability, but only in some of the patient-derived lines. Likewise, effects of HA concentration on 3D invasion also varied across patient-derived cell lines. This finding is expected given the high degree of interpatient heterogeneity in GBM clinical pathology.[103] Notably, cell invasiveness in response to HA concentration or ezrin inhibition was not uniform across GBM tumor subtypes, as previously defined.[70,71] This is not unexpected, as there is no clear evidence that these subtypes impact clinical outcomes and given single-cell RNA sequencing analysis of primary clinical tumors, which indicates that no tumor is truly a single subtype.[104] Thus, the 3D culture platform presented here may have utility to identify patient-specific responses to therapeutics, such as those targeting migration, to inform personalized clinical strategies.

A number of studies have suggested that the small molecule ezrin inhibitor used in these studies, NSC668394, may have value as a clinical cancer therapy,[39,41] but no clinical trials evaluating NSC668394 have been registered on ClinicalTrials.gov at this time. In general, results from this study support the therapeutic potential of NSC668394 for GBM, as in most patient lines and matrix conditions NSC668394 reduced cancer cell survival and migration. While NSC668394 treatment inhibited GS invasion in conditions with high degrees of tethering of the HA matrix to the cytoskeleton, in matrices with minimal levels of HA–CD44 binding low doses of NSC668394 increased

Figure 6. Greater CD44–ezrin colocalization occurs in more migratory GSs. A) Representative images of HK408 GSs stained for CD44 and ezrin following 6 days of culture. Scale bars = 10 μm. B) Representative images of GS054 GSs stained for CD44 and ezrin following 6 days of culture. Scale bars = 10 μm. C) Pearson correlation coefficient distribution of overlapping CD44 and ezrin in staining for HK408 GSs. D) Pearson correlation coefficient distribution of overlapping CD44 and ezrin in staining for GS054 GSs. Kruskal–Wallis statistical test was used followed by post-hoc Dunn's multiple comparisons test of significance. *$p < 0.05$; ***$p < 0.001$; ****$p < 0.0001$.

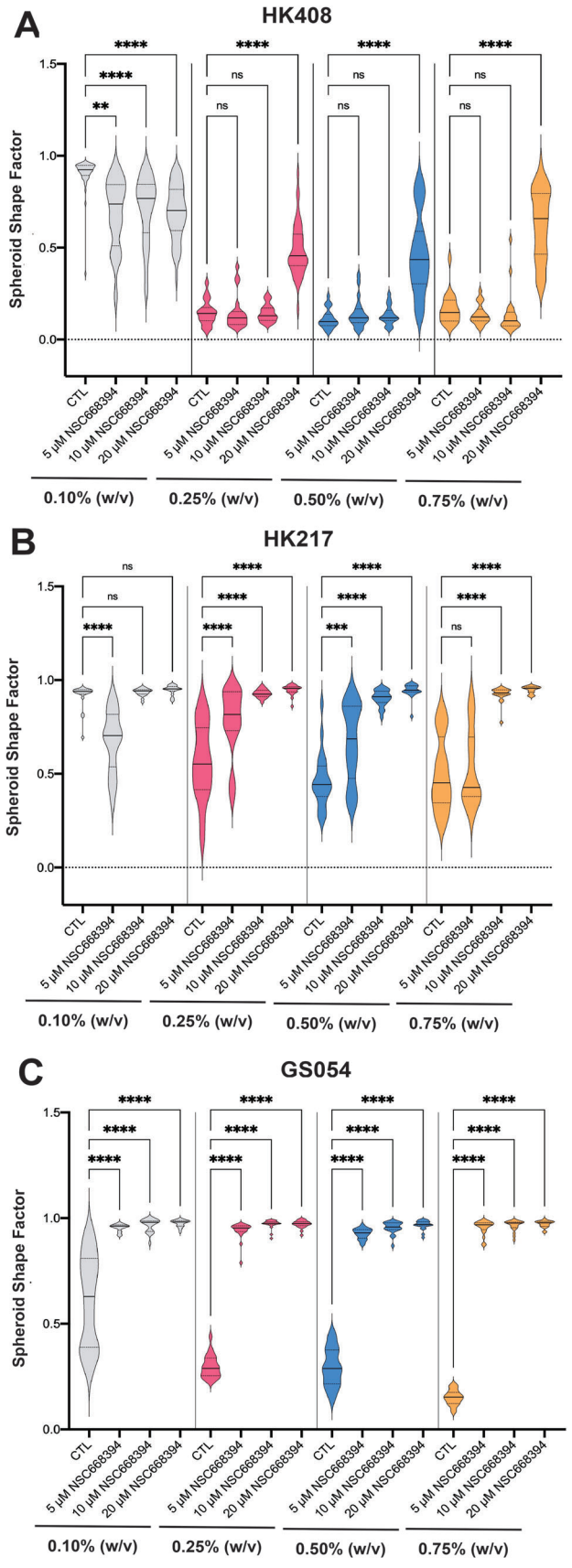

migration of cells using what appears to be an amoeboid-like mode. In all conditions, larger doses of NSC668394 induced apoptosis and prevented migration.

Overall, results support the idea that inhibiting ezrin phosphorylation is a promising therapeutic strategy for GBM; however, delivering subtherapeutic doses may result in only partial blocking or even stimulation of tumor cell invasion, depending on the local ECM. In addition, results suggest that further studies investigating efficacy of NSC668394 as a co-therapy with cilengitide, a competitive antagonist for integrin binding to RGD-bearing ECM proteins, are warranted. While cilengitide has shown promise in preclinical and clinical trials, efficacy was not clear in phase 3 trials.[105] However, it is possible in some cases that CD44–ezrin mediated migration of GBM cells may compensate for reduced integrin adhesion with cilengitide treatment.

Beyond findings reported here, there remain several areas to be investigated, including the roles of matrix degradation, other proteins known to link CD44 to the actin cytoskeleton, non-ezrin proteins in the ERM complex, and other potentially redundant signaling pathways. In this study, the 3D culture scaffolds used contained no matrix metalloprotease-degradable sites but were susceptible to hyaluronidase degradation. Thus, matrices with lower HA content are inherently more degradable than those with higher HA content. While differences in HA degradation could certainly affect migratory capacity, data clearly show that HA–CD44 interactions facilitate transduction of forces needed for migration. HA molecular weight is another factor that affects CD44 signaling and cell migration.[106] However, the current studies used only high molecular HA (≈700 kDa, similar to HA in native brain tissue,[55]) so that effects of HA concentration on GBM cells could be isolated.

Moreover, there are proteins other than ezrin known to link CD44 to the actin cytoskeleton, including ankyrin and IQAPI, which have previously been suggested to mediate cell migration.[87,107] However, it is unclear if these adapter proteins have redundant, agonistic, or antagonist actions to ezrin. In addition, while NSC668394 has been previously identified as a potent inhibitor of ezrin phosphorylation, it may have off-target effects on radixin and moesin. Finally, several other signaling proteins involved in migration, such as ERK/MAPK, PKC, and RhoA/ROCK, create complex interactions and feedback loops to integrate matrix signals transduced through integrins and CD44 and regulate migration.[12,108,109] Thus, it will be important in future studies to take a systems-level approach to understand how cells integrate biochemical and mechanical cues from their matrix to enable migration.

4. Conclusions

Here, we used soft, 3D matrices designed to approximate the peritumoral microenvironment of GBM tumors to investigate how HA in the ECM affects cancer cell invasion. In general, results

Figure 7. Effects of NSC669384 on GS migration. Spheroid shape factor distribution of A) HK408, B) HK217, and C) GS054 GSs at endpoint following treatment with 0–20 μM of NSC669384. Kruskal–Wallis ANOVA statistical test was used followed by post-hoc Dunn's multiple comparisons test of significance. $^{**}p < 0.01$; $^{***}p < 0.001$; $^{****}p < 0.0001$.

show that GBM cell invasion has a biphasic dependence on HA concentration, supporting the concept that GBM cell migration follows the "motor-clutch" model of cell migration, where CD44-ERM complexes act as molecular clutches to regulate the extent of migratory activity independently of integrin attachments. Results also support previous findings that CD44–ezrin complexes act as "pickets," as defined in the anchored "picket-fence" model, where migration requires dynamic, spatiotemporal coordination of anchoring and releasing of "pickets" though ezrin phosphorylation and dephosphorylation, for migration to occur. Inhibition of ezrin activation through NSC668394 represents a promising strategy for preventing GBM cell invasion. However, in very soft tissue microenvironments, where cells can bind the matrix via integrins but not CD44, low-level NSC668394 doses may induce a phenotypic switch in GBM cells from a mesenchymal-like to an ameboid-like migration state, presenting a means of therapeutic resistance.

5. Experimental Section

HA Thiolation and Hydrogel Fabrication: Approximately 4.5–6% of D-glucuronic acid carboxylic acid groups in the repeating HA disaccharide chain (M_W = 700 kDa, LifeCore Biomedical) were thiolated via carbodiimide chemistry (*N*-hydroxysuccinimide; 1-ethyl-3-[3-dimethylaminopropyl] [EDC]) and reaction with cysteamine (Sigma-Aldrich) to yield HA-SH. Following reduction with dithiothreitol and subsequent dialysis for purification, proton nuclear magnetic resonance spectroscopy and an Ellman's test were conducted to verify HA-SH thiolation percentage.

Prior to gelation, compounds were buffered in 4-(2-hydroxyethyl)-1-piperazineethanesulfonic acid (HEPES; Fischer BioReagents) with Hank's buffer salt solution (Sigma-Aldrich) to yield the following solution densities: 10 mg mL^{-1} HA-SH; 100 mg mL^{-1} thiol-terminated 4-arm polyethylene glycol (PEG-SH, M_W = 20 kDa, Laysan Bio); 100 mg mL^{-1} 8-arm polyethylene glycol norbornene (PEG-Norb; M_W = 20 kDa, Laysan Bio); 4 mM thiolated RGD peptide (RGD-SH, 'GCGYGRGDSPG'; GenScript); 1–3 mg mL^{-1} Lithium phenyl-2,4,6-trimethylbenzoylphosphinate (LAP; Sigma-Aldrich). Prepared gel solutions contained 0.25% w/v LAP, 0.25 mM RGD-SH, and either 0.10%, 0.25%, 0.50%, or 0.75% w/v of HA-SH.

30 µL of finalized gel solutions were added to 30 mm^3 cylindrical slots in silicone molds. These solutions were then exposed to 3.95–4.05 mW cm^{-2} magnitude of 365 nm UV radiation for 15 s to initiate gelation. Gel products were removed from molds and maintained in PBS (D-PBS) until characterization.

Hydrogel Characterization: *Mechanical property testing*: Hydrogel storage moduli (G') were measured using a discovery hybrid rheometer-2 (DHR-2, TA Instruments) at 37 °C. Frequency sweeps were performed under 1% constant strain in the range of 0.1–1.0 Hz. Storage modulus of each sample was calculated as the average value of the linear region of the storage curve from the frequency sweep plot. For statistical analysis, three separate measurements were taken in which five samples from each condition were measured.

Mass-swelling ratio: Fabricated hydrogels without cells were weighed using a scale (Weight$_{i,1}$) and subsequently incubated in 1× PBS at 37 °C and 5% CO_2. After 24 h, the weight of each hydrogel was again recorded (Weight$_{i,2}$). The formula below was used to calculate the mass swelling ratio per hydrogel.

$$\text{Mass Swelling Ratio} = \frac{\text{Weight}_{i,2}}{\text{Weight}_{i,1}} \tag{1}$$

Diffusion modeling: For diffusion measurements, FRAP was used. Hydrogels were incubated with FITC–Dextran solution (0.33 mg mL^{-1} in PBS) overnight. Five pre-bleach images were taken at 10% power of a 488 nm laser under a SP5 laser scanning confocal microscope (Leica). In order to photo-bleach the samples, 30 µm region of hydrogels were exposed to a 488 nm laser (600 µm pinhole) for 20 s. 1000 frame of images were taken as post bleached images. t_d values (time for half recover) were calculated from fluorescence recovery graphs. Diffusion coefficients (D_e) were calculated using simplified Fick's law:[110]

$$\frac{M_t}{M_{inf}} = 2\left[\frac{D_e t}{\pi x^2}\right]^{1/2} \tag{2}$$

Patient-Derived GBM Cell Culture: GS054, HK177, HK217, and HK408 were the patient-derived GBM lines used in this study. Patient line GS54 (passages 14–18) and lines HK177 (passages 15–17), HK217 (passages 11–22), and HK408 (passages 15–24) were generously provided by Dr. David Nathanson (UCLA, GS54) and Dr. Harley Kornblum (UCLA, HK lines), respectively. While all patient lines were sphere-forming, HK217, HK177, and GS54 cells were expanded in suspension cultured while HK408 cells were expanded as monolayers. All cells were collected in adherence to the UCLA Institutional Review Board and provided with no identifying information. All GBM cells were cultured in T-75 flasks with complete media which consisted of DMEM/F12 with L-glutamine and 15 mM HEPES in 1× Gem21, 0.2% Normocin, 20 ng mL^{-1} human fibroblast growth factor-2, 50 ng mL^{-1} human epidermal growth factor, and 25 mg mL^{-1} heparin. Both 2D and 3D cultures were incubated in 5% CO_2 and 37 °C throughout the course of all experiments. For passaging, 1× TrypLE (Life Technologies) was used for GS dissociation or monolayer disruption. Single cells were replated at 100 000 cells mL^{-1} to establish subcultures.

Gliomasphere Culture and 3D Encapsulation: Following passaging, single GBM cells were seeded (600 000 cells/well) into individual wells of a 24-well AggreWell plate pre-coated with 5% Pluronic in 1× PBS solution. Centrifugation (300 × *g* for 3 min) and incubation (5% CO_2 and 37 °C) followed. After 18 h, GSs were prepared for suspension culture or 3D encapsulation within hydrogels. For 3D encapsulation, GSs, ≈150 µm in diameter, were harvested from AggreWell plates and resuspended in prepared gel solutions (0.10–0.75% w/v) (see "HA Thiolation and Hydrogel Fabrication"). Gelation of mixed gel and GS solutions ensued as previously described in the methods and yielded the 3D hydrogels containing the patient-derived GBM spheroids at a density of 100 GSs per 30 µL of hydrogel.

Microscopy and Quantification of Invasion: Phase contrast images were obtained using the Zeiss Axio-Observer microscope and Zen software, and image analysis was performed using the ImageJ software. GS invasion was quantified by spheroid shape factor, a ratio of a GS's area to its squared perimeter, and migration length, the maximum protrusion radius from a GS's periphery. Perimeter (*P*) and area (*A*) values were obtained by manually tracing GSs, and spheroid shape factor was calculated using the following formula:

$$\text{Spheroid Shape Factor} = \frac{4\pi A}{P^2} \tag{3}$$

Cryopreservation, Immunostaining, and Confocal Imaging: Hydrogels underwent fixation in 4% paraformaldehyde (PFA) in 1× PBS solution for 1 h at room temperature. Then, it was followed by sequential incubations in solutions of 5% and 20% sucrose in 1× PBS for 1 h time periods. After leaving the hydrogels in 20% sucrose solutions overnight at 4 °C, hydrogels were embedded in 20% sucrose in preservation molds containing 1× optimal cutting temperature compound for 3 h at 4 °C and flash frozen in 2-methylbutane. Frozen hydrogels were cut into 12 mm sections using the Leica Cryostat.

Sections were fixed in 4% PFA in 1× PBS solution for 12 min before being subsequently washed using 0.10% Tween-20 in 1× tris-buffered saline (TBS-T) and blocked with 4% bovine serum albumin (BSA) in 1× TBS-T for 1 h in room temperature. Then, sections were incubated at 4 °C overnight with primary antibodies for CD44 (1:400, 37259T, Cell Signaling Technology), RHAMM (1:400, NBP1-76538, Novus Biologicals), Ezrin (1:200, 3145S, Cell Signaling Technology), Ki67 (1:100, PA5-16785, Invit-

rogen), and cleaved PARP (1:400, 5625S, Cl-PARP, Cell Signaling Technology) or biotinylated HA binding protein (1:100, 385911-50UG, HA binding peptide [HABP], EMD Millipore) diluted in blocking solution according to the provided manufacturer's recommendations. The next day, samples were incubated in Hoechst 33342 and appropriate secondary antibody solutions with limited light exposure for 1 h. Following a final wash, slides were mounted using coverslips with applied Fluoromount G (Southern Biotech, Birmingham, AL, USA) and imaged using confocal microscopy.

Cell Extraction from Hydrogels and EdU Proliferation Assay: Cultured and encapsulated spheres were incubated in a 1:1000 dilution of EdU solution (Cayman Chemical Company) for 4 h. Following a wash in PBS, hydrogel samples were broken down using a 10 mL syringe with a 20G needle and passed through a 40 mm filter into collection tubes. For 2D culture, GBM spheres were disintegrated using TrypIE before further processing. All samples were subsequently centrifuged (400 × *g* for 5 min), resuspended in 4% PFA in 1× PBS, and stored in 4 °C overnight.

The following day, samples were centrifuged (400 × *g* for 5 min) and washed in 1% BSA in 1× PBS. Cells were permeabilized for 15 min in permeabilization buffer (0.1% Saponin and 1% BSA in 1× PBS). Staining solution was prepared and added to the cells undergoing the permeabilization reaction. After 30 min of incubation without light in room temperature, samples were washed twice and ultimately resuspended in permeabilization buffer. Flow cytometry data were collected using the Guava easyCyte flow cytometer and analyzed using FlowJo software.

Cell Viability Quantification: Encapsulated GSs were incubated at 37 °C and 5% CO_2 for 15 min in LIVE/DEAD working reagent prepared by diluting 2 mM ethidium homodimer-1 (1:500) and 4 mM calcein AM solution (1:2000) stock solutions in 1× PBS. Spheres were imaged and three separate counters quantified the presence of live or dead cells in images provided.

Tissue Microarray HA Staining and Scoring: TMAs were prepared by clinically isolated tissue biopsy samples from 39 GBM and 19 lower-grade CNS cancer (grade I-III astrocytoma, grade I-III oligodendroglioma, pituitary gland cancer, and meningioma) patients, prepared and provided with no individually identifying information by the UCLA Brain Tumor Tissue Resource, which was under the direction of Dr. William Yong who had full approval of UCLA Institutional Review Board to obtain and share de-identified samples. Paraffin-embedded slides of 5 mm thickness were de-paraffined using 100% xylene and a five-step reduction in alcohol presentation from 100% ethanol to deionized water. Samples were washed (0.1% Tween in 1× TBS), blocked (5% normal goat serum and 1% BSA in washing solution), and incubated with biotinylated HABP overnight at 4 °C. The following day, samples were washed and incubated using Vectastain ABC kit reagents and 3,3′-diaminobenzidine substrate. Samples were mounted onto slides using a toluene solution. Images were taken using the Zen Axio-Observer microscope and images were semi-quantitatively scored according to a previously described method.[111]

In Vivo Intracranial Xenograft Tumor Models: 8-week-old female NOD SCID gamma null mice (NSG) were used for GBM intracranial implantation. All animal experiments were carried out under an Institutional Animal Research Committee (ARC) (ARC-1993-285) approved protocol according to NIH guidelines at the University of California, Los Angeles. The GSCs suspension (2×10^5 cells in 3 µL of PBS) was injected into the brains of NSG mice as previously described.[112] When mice developed neuropathological symptoms, they were sacrificed and perfused with ice-cold PBS followed by 4% PFA. Mice brains were dissected and fixed in 4% PFA for 24 h. The brains were then transferred to 10% formalin and processed for subsequent histopathological analysis.

Statistics: All statistics were performed using GraphPad Prism software. Kolmogorov–Smirnov test was performed to assess normality of data. For parametric data, a Student's *t*-test and one- or two-way analysis of variance (ANOVA) was performed to assess significance between two and multiple data sets, respectively, followed by post-hoc Tukey's multiple comparisons test. In the case of non-parametric data, a Kruskal–Wallis ANOVA was used to assess significant differences between any data sets followed by post-hoc Dunn's multiple comparisons test. Modes of significance were reported as follows: ns, non-significant; *, $p < 0.05$; **, $p < 0.01$; ***, $p < 0.001$; ****, $p < 0.0001$.

Supporting Information

Supporting Information is available from the Wiley Online Library or from the author.

Acknowledgements

Confocal laser scanning microscopy was performed at the Advanced Light Microscopy/Spectroscopy Laboratory and the Leica Microsystems Center of Excellence at the California NanoSystems Institute at UCLA with funding support from NIH Shared Instrumentation Grant S10D025017 and NSF Major Research Instrumentation grant CHE-0722519. The authors thank Dr. David Nathanson for providing patient-derived cells and Dr. William Yong for providing tissue microarray slides. Funding for this work was generously provided by the NIH (R01 CA241927-01A1, R21NS093199, S.K.S.) and an American Brain Tumor Association Discovery grant (S.K.S.).

Conflict of Interest

The authors declare no conflict of interest.

Author Contributions

G.S., A.S., and I.S. contributed equally to this work. Concept and design: G.S., A.S., I.S., H.I.K., and S.K.S.; Methodology development: G.S., A.S., I.S., W.X., and S.K.S.; Data acquisition: G.S., A.S., I.S., S.B., B.W.R., and M.C.C.; Data analysis and interpretation: G.S., A.S., I.S., M.E., I.R., K.T., B.S., J.H., M.J.H., T.S., and S.K.S.; Manuscript writing and revisions: G.S., A.S., S.B., and S.K.S.; Study supervision: H.I.K. and S.K.S.

Data Availability Statement

The data that support the findings of this study are available from the corresponding author upon reasonable request.

Keywords

CD44, ezrin, glioblastoma, hyaluronic acids, hydrogels

Received: December 3, 2022
Published online: February 8, 2023

[1] A. C. Tan, D. M. Ashley, G. Y. López, M. Malinzak, H. S. Friedman, M. Khasraw, *CA Cancer J. Clin* **2020**, *70*, 299.
[2] A. A. Puca, V. Lopardo, F. Montella, P. Di Pietro, D. Cesselli, I. G. Rolle, M. Bulfoni, V. Di Sarno, G. Iaconetta, P. Campiglia, C. Vecchione, A. P. Beltrami, E. Ciaglia, *Cells* **2022**, *11*, 294.
[3] R. Stupp, W. P. Mason, M. J. Van Den Bent, M. Weller, B. Fisher, M. J. B. Taphoorn, K. Belanger, A. A. Brandes, C. Marosi, U. Bogdahn, J. Curschmann, R. C. Janzer, S. K. Ludwin, T. Gorlia, A. Allgeier, D. Lacombe, J. G. Cairncross, E. Eisenhauer, R. O. Mirimanoff, *N. Engl. J. Med.* **2005**, *352*, 987.
[4] A. F. Tamimi, M. Juweid, in *Glioblastoma* (Ed: S. De Vleeschouwer), Codon Publications, Brisbane, AU **2017**, pp. 143–153.
[5] G. Shukla, G. S. Alexander, S. Bakas, R. Nikam, K. Talekar, J. D. Palmer, W. Shi, *Chin Clin Oncol* **2017**, *6*, 40.
[6] T. Chouleur, M. L. Tremblay, A. Bikfalvi, *Curr Opin Oncol* **2020**, *32*, 631.

[7] H. J. Scherer, *J Neurol Psychiatry* **1940**, *3*, 147.
[8] G. Abatangelo, V. Vindigni, G. Avruscio, L. Pandis, P. Brun, *Cells* **2020**, *9*, 7.
[9] M. Valkonen, H. Haapasalo, K. Rilla, K. Tyynelä-Korhonen, Y. Soini, S. Pasonen-Seppänen, *BMC Cancer* **2018**, *18*, 664.
[10] L. Jadin, S. Pastorino, R. Symons, N. Nomura, P. Jiang, T. Juarez, M. Makale, S. Kesari, *Ann. Transl. Med.* **2015**, *3*, 80.
[11] S. Misra, V. C. Hascall, R. R. Markwald, S. Ghatak, *Front Immunol* **2015**, *6*, 201.
[12] J. B. Park, H. J. Kwak, S. H. Lee, *Cell Adh Migr* **2008**, *2*, 202.
[13] B. L. Bangasser, D. J. Odde, *Cell. Mol. Bioeng.* **2013**, *6*, 449.
[14] E. M. Craig, J. Stricker, M. Gardel, A. Mogilner, *Phys Biol* **2015**, *12*, 035002.
[15] C. E. Chan, D. J. Odde, *Science* **2008**, *322*, 1687.
[16] P. A. DiMilla, K. Barbee, D. A. Lauffenburger, *Biophys. J.* **1991**, *60*, 15.
[17] S. R. Peyton, A. J. Putnam, *J. Cell. Physiol.* **2005**, *204*, 198.
[18] A. Pathak, *Phys Biol* **2018**, *15*, 065001.
[19] R. L. Klank, S. A. D. Grunke, B. L. Bangasser, C. L. Forster, M. A. Price, T. J. Odde, K. S. Santacruz, S. S. Rosenfeld, P. Canoll, E. A. Turley, J. B. Mccarthy, J. R. Ohlfest, D. J. Odde, *Cell Rep.* **2017**, *18*, 23.
[20] C. J. Liu, G. A. Shamsan, T. Akkin, D. J. Odde, *Biophys. J.* **2019**, *117*, 1179.
[21] L. S. Prahl, P. F. Bangasser, L. E. Stopfer, M. Hemmat, F. M. White, S. S. Rosenfeld, D. J. Odde, *Cell Rep.* **2018**, *25*, 2591.
[22] Y. Kim, S. Kumar, *Mol. Cancer Res.* **2014**, *12*, 1416.
[23] B. L. Bangasser, S. S. Rosenfeld, D. J. Odde, *Biophys. J.* **2013**, *105*, 581.
[24] A. Macdonald, A. R. Horwitz, D. A. Lauffenburger, *Cell Adh Migr* **2008**, *2*, 95.
[25] L. B. Case, C. M. Waterman, *Nat. Cell Biol.* **2015**, *17*, 955.
[26] T. A. Martin, G. Harrison, R. E. Mansel, W. G. Jiang, *Crit. Rev. Oncol. Hematol.* **2003**, *46*, 165.
[27] S. Tsukita, K. Oishi, N. Sato, J. Sagara, A. Kawai, S. Tsukita, *J. Cell Biol.* **1994**, *126*, 391.
[28] A. García-Ortiz, J. M. Serrador, *Int. J. Mol. Sci.* **2020**, *21*, 1502.
[29] Y. Liu, N. V. Belkina, C. Park, R. Nambiar, S. M. Loughhead, G. Patino-Lopez, K. Ben-Aissa, J.-J. Hao, M. J. Kruhlak, H. Qi, U. H. Von Andrian, J. H. Kehrl, M. J. Tyska, S. Shaw, *Blood* **2012**, *119*, 445.
[30] G. Giannone, R. M. Mège, O. Thoumine, *Trends Cell Biol.* **2009**, *19*, 475.
[31] Z. Razinia, P. Castagnino, T. Xu, A. Vázquez-Salgado, E. Puré, R. K. Assoian, *Stem Cells Int* **2017**, *7*, 1.
[32] W. Xiao, S. Wang, R. Zhang, A. Sohrabi, Q. Yu, S. Liu, A. Ehsanipour, J. Liang, R. D. Bierman, D. A. Nathanson, S. K. Seidlits, *Matrix Biol.* **2020**, *85–86*, 128.
[33] A. Kusumi, C. Nakada, K. Ritchie, K. Murase, K. Suzuki, H. Murakoshi, R. S. Kasai, J. Kondo, T. Fujiwara, *Annu. Rev. Biophys. Biomol. Struct.* **2005**, *34*, 351.
[34] J. M. Kalappurakkal, P. Sil, S. Mayor, *Protein Sci.* **2020**, *29*, 1355.
[35] S. A. Freeman, A. Vega, M. Riedl, R. F. Collins, P. P. Ostrowski, E. C. Woods, C. R. Bertozzi, M. I. Tammi, D. S. Lidke, P. Johnson, S. Mayor, K. Jaqaman, S. Grinstein, *Cell* **2018**, *172*, 305.
[36] T. Gabay, E. Jakobs, E. Ben-Jacob, Y. Hanein, *Phys. A* **2005**, *350*, 611.
[37] S. Donatello, I. S. Babina, L. D. Hazelwood, A. D. K. Hill, I. R. Nabi, A. M. Hopkins, *Am. J. Pathol.* **2012**, *181*, 2172.
[38] A. Ghaffari, V. Hoskin, G. Turashvili, S. Varma, J. Mewburn, G. Mullins, P. A. Greer, F. Kiefer, A. G. Day, Y. Madarnas, S. Sengupta, B. E. Elliott, *Breast Cancer Res.* **2019**, *21*, 12.
[39] G. Bulut, S.-H. Hong, K. Chen, E. M. Beauchamp, S. Rahim, G. W. Kosturko, E. Glasgow, S. Dakshanamurthy, H.-S. Lee, I. Daar, J. A. Toretsky, C. Khanna, A. Üren, *Oncogene* **2011**, *31*, 269.
[40] M. Paige, G. Kosturko, G. Bulut, M. Miessau, S. Rahim, J. A. Toretsky, M. L. Brown, A. Üren, *Bioorg. Med. Chem.* **2014**, *22*, 478.
[41] A. Proudfit, N. Bhunia, D. Pore, Y. Parker, D. Lindner, N. Gupta, *Sarcoma* **2020**, *2020*, 9010496.
[42] Y. Song, X. Ma, M. Zhang, M. Wang, G. Wang, Y. Ye, W. Xia, *Front Cell Dev Biol* **2020**, *8*, 1321.
[43] J. J. Qin, J. M. Wang, J. Du, C. Zeng, W. Han, Z. D. Li, J. Xie, G. L. Li, *Asian Pac. J. Cancer Prev.* **2014**, *15*, 9805.
[44] X. Zhu, F. C. Morales, N. K. Agarwal, T. Dogruluk, M. Gagea, M. M. Georgescu, *Cancer Res.* **2013**, *73*, 1142.
[45] C. Wang, X. Tong, F. Yang, *Mol. Pharmaceutics* **2014**, *11*, 2115.
[46] J. Cha, S. G. Kang, P. Kim, *Sci. Rep.* **2016**, *6*, 1.
[47] S. Pedron, E. Becka, B. A. C. Harley, *Biomaterials* **2013**, *34*, 7408.
[48] K. J. Wolf, S. Lee, S. Kumar, *APL Bioeng.* **2018**, *2*, 031903.
[49] B. Ananthanarayanan, Y. Kim, S. Kumar, *Biomaterials* **2011**, *32*, 7913.
[50] J. W. E. Chen, S. Pedron, P. Shyu, Y. Hu, J. N. Sarkaria, B. A. C. Harley, *Front. Mater.* **2018**, *5*, 39.
[51] Y. A. Miroshnikova, J. K. Mouw, J. M. Barnes, M. W. Pickup, J. N. Lakins, Y. Kim, K. Lobo, A. I. Persson, G. F. Reis, T. R. Mcknight, E. C. Holland, J. J. Phillips, V. M. Weaver, *Nat. Cell Biol.* **2016**, *18*, 1336.
[52] W. Xiao, R. Zhang, A. Sohrabi, A. Ehsanipour, S. Sun, J. Liang, C. M. Walthers, L. Ta, D. A. Nathanson, S. K. Seidlits, *Cancer Res.* **2018**, *78*, 1358.
[53] J. M. Cyphert, C. S. Trempus, S. Garantziotis, *Int J Cell Biol* **2015**, *2015*, 563818.
[54] A. G. Tavianatou, I. Caon, M. Franchi, Z. Piperigkou, D. Galesso, N. K. Karamanos, *FEBS J.* **2019**, *286*, 2883.
[55] Z. Z. Khaing, B. D. Milman, J. E. Vanscoy, S. K. Seidlits, R. J. Grill, C. E. Schmidt, *J. Neural Eng.* **2011**, *8*, 046033.
[56] G. Kogan, L. Šoltés, R. Stern, P. Gemeiner, *Biotechnol. Lett.* **2007**, *29*, 17.
[57] M. K. Cowman, H. G. Lee, K. L. Schwertfeger, J. B. McCarthy, E. A. Turley, *Front Immunol* **2015**, *6*, 261.
[58] B. Delpech, C. Maingonnat, N. Girard, C. Chauzy, A. Olivier, R. Maunoury, J. Tayot, P. Creissard, *Eur J Cancer* **1993**, *29*, 1012.
[59] Y. Cui, S. Cole, J. Pepper, J. J. Otero, J. O. Winter, *Biomater. Sci.* **2020**, *8*, 4821.
[60] X. Wang, T. Lou, W. Zhao, G. Song, C. Li, G. Cui, *J. Biomater. Appl.* **2016**, *30*, 1545.
[61] B. L. Bangasser, G. A. Shamsan, C. E. Chan, K. N. Opoku, E. Tüzel, B. W. Schlichtmann, J. A. Kasim, B. J. Fuller, B. R. Mccullough, S. S. Rosenfeld, D. J. Odde, *Nat. Commun.* **2017**, *8*, 15313.
[62] B. Delpech, C. Maingonnat, N. Girard, C. Chauzy, A. Olivier, R. Maunoury, J. Tayot, P. Creissard, *Eur J Cancer* **1993**, *29A*, 1012.
[63] B. Glimelius, B. Norling, B. Westermark, A. Wasteson, *Biochem. J.* **1978**, *172*, 443.
[64] B. Glimelius, B. Norling, B. Westermark, A. Wasteson, *J. Cell. Physiol.* **1979**, *98*, 527.
[65] J. Liang, A. Sohrabi, M. Epperson, L. M. Rad, T. Kelly, M. Sathialingam, T. Skandakumar, P. Lue, J. Huang, J. Popoli, A. Yackly, M. Bick, *J Vis Exp* **2022**, *184*, e63791.
[66] J. Weickenmeier, R. de Rooij, S. Budday, P. Steinmann, T. C. Ovaert, E. Kuhl, *Acta Biomater.* **2016**, *42*, 265.
[67] S. Budday, T. C. Ovaert, G. A. Holzapfel, P. Steinmann, E. Kuhl, *Arch. Comput. Methods Eng.* **2019**, *27*, 1187.
[68] J. Necas, L. Bartosikova, P. Brauner, J. Kolar, *Vet. Med.* **2008**, *53*, 397.
[69] T. A. Dechert, A. E. Ducale, S. I. Ward, D. R. Yager, *Wound Repair Regen* **2006**, *14*, 252.
[70] R. G. W. Verhaak, K. A. Hoadley, E. Purdom, V. Wang, Y. Qi, M. D. Wilkerson, C. R. Miller, L. Ding, T. Golub, J. P. Mesirov, G. Alexe, M. Lawrence, M. O'kelly, P. Tamayo, B. A. Weir, S. Gabriel, W. Winckler, S. Gupta, L. Jakkula, H. S. Feiler, J. G. Hodgson, C. D. James, J. N. Sarkaria, C. Brennan, A. Kahn, P. T. Spellman, R. K. Wilson, T. P. Speed, J. W. Gray, M. Meyerson, et al., *Cancer Cell* **2010**, *17*, 98.

[71] D. R. Laks, T. J. Crisman, M. Y. S. Shih, J. Mottahedeh, F. Gao, J. Sperry, M. C. Garrett, W. H. Yong, T. F. Cloughesy, L. M. Liau, A. Lai, G. Coppola, H. I. Kornblum, *Neuro Oncol* **2016**, *18*, 1367.
[72] S. Pedron, G. L. Wolter, J. W. E. Chen, S. E. Laken, J. N. Sarkaria, B. A. C. Harley, *Biomaterials* **2019**, *219*, 119371.
[73] E. Wang, Q. Li, H. Gao, H. Xu, X. Wang, Y. Pan, F. Hao, X. Qiu, M. Stoecker, E. Wang, *Tumour Biol* **2012**, *33*, 1493.
[74] M. Kijewska, M. Kocyk, M. Kloss, K. Stepniak, Z. Korwek, R. Polakowska, M. Dabrowski, A. Gieryng, B. Wojtas, I. A. Ciechomska, B. Kaminska, *OncoTargets Ther.* **2017**, *8*, 16340.
[75] G. Charras, E. Paluch, *Nat. Rev. Mol. Cell Biol.* **2008**, *9*, 730.
[76] E. K. Paluch, E. Raz, *Curr. Opin. Cell Biol.* **2013**, *25*, 582.
[77] T. Lämmermann, M. Sixt, *Curr. Opin. Cell Biol.* **2009**, *21*, 636.
[78] V. Graziani, I. Rodriguez-Hernandez, O. Maiques, V. Sanz-Moreno, *Trends Cell Biol.* **2022**, *32*, 228.
[79] R. Golshani, L. Lopez, V. Estrella, M. Kramer, N. Iida, V. B. Lokeshwar, *Cancer Res.* **2008**, *68*, 483.
[80] S. S. Khurana, T. E. Riehl, B. D. Moore, M. Fassan, M. Rugge, J. Romero-Gallo, J. Noto, R. M. Peek, W. F. Stenson, J. C. Mills, *J. Biol. Chem.* **2013**, *288*, 16085.
[81] C. Chen, S. Zhao, A. Karnad, J. W. Freeman, *J. Hematol. Oncol.* **2018**, *11*, 1.
[82] C. C. Lin, A. Raza, H. Shih, *Biomaterials* **2011**, *32*, 9685.
[83] C. Wang, S. Sinha, X. Jiang, L. Murphy, S. Fitch, C. Wilson, G. Grant, F. Yang, *Tissue Eng., Part A* **2021**, *27*, 390.
[84] S. Pedron, B. A. C. Harley, *J. Biomed. Mater. Res., Part A* **2013**, *101*, 3404.
[85] S. K. Seidlits, Z. Z. Khaing, R. R. Petersen, J. D. Nickels, J. E. Vanscoy, J. B. Shear, C. E. Schmidt, *Biomaterials* **2010**, *31*, 3930.
[86] Y. Kim, S. Kumar, *Mol. Cancer Res.* **2014**, *12*, 1416.
[87] K. J. Wolf, P. Shukla, K. Springer, S. Lee, J. D. Coombes, C. J. Choy, S. J. Kenny, K. Xu, S. Kumar, *Proc. Natl. Acad. Sci. USA* **2020**, *117*, 11432.
[88] W. Xiao, A. Ehsanipour, A. Sohrabi, S. K. Seidlits, *J Vis Exp* **2018**, *2018*, e58176.
[89] U. Ben-David, R. Beroukhim, T. R. Golub, *Nat. Rev. Cancer* **2019**, *19*, 97.
[90] G. Kaur, J. M. Dufour, *Spermatogenesis* **2012**, *2*, 1.
[91] J. S. Rao, P. A. Steck, P. Tofilon, D. Boyd, F. Ali-Osman, W. G. Stetler-Stevenson, L. A. Liotta, R. Sawaya, *J. Neuro-Oncol.* **1993**, *18*, 129.
[92] K. Wei, C. Huang, P. Chen, L. Feng, T. E. Wu, S. Chen, H. Tsai, Y. Lu, N. Tsang, C. Tseng, P. Pai, J. Shin, *Anticancer Res.* **2010**, *30*, 253.
[93] R. F. Lamb, B. W. Ozanne, C. Roy, L. McGarry, C. Stipp, P. Mangeat, D. G. Jay, *Curr. Biol.* **1997**, *7*, 682.
[94] B. M. Marsick, J. E. S. Miguel-Ruiz, P. C. Letourneau, *J. Neurosci.* **2012**, *32*, 282.
[95] P. Mrass, I. Kinjyo, L. G. Ng, S. L. Reiner, E. Puré, W. Weninger, *Immunity* **2008**, *29*, 971.
[96] M. Ma, M. Baumgartner, *PLoS One* **2013**, *8*, e75577.
[97] N. Parameswaran, K. Matsui, N. Gupta, *J. Immunol.* **2011**, *186*, 4088.
[98] P. Sil, N. Mateos, S. Nath, S. Buschow, C. Manzo, K. G. N. Suzuki, T. Fujiwara, A. Kusumi, M. F. Garcia-Parajo, S. Mayor, *Mol. Biol. Cell* **2020**, *31*, 561.
[99] Z. N. Zhou, P. J. Boimel, J. E. Segall, *Drug Discov Today* **2011**, *8*, 95.
[100] F. Y. Lim, Y. L. Koon, K. H. Chiam, *Comput Methods Biomech Biomed Engin* **2013**, *16*, 1085.
[101] Y. J. Liu, M. Le Berre, F. Lautenschlaeger, P. Maiuri, A. Callan-Jones, M. Heuzé, T. Takaki, R. Voituriez, M. Piel, *Cell* **2015**, *160*, 659.
[102] R. J. Jerrell, M. J. Leih, A. Parekh, *Small GTPases* **2020**, *11*, 131.
[103] N. R. Parker, P. Khong, J. F. Parkinson, V. M. Howell, H. R. Wheeler, *Front Oncol* **2015**, *5*, 55.
[104] A. H. Martínez, R. Madurga, N. García-Romero, Á. Ayuso-Sacido, *Cancer Lett* **2022**, *527*, 66.
[105] R. Stupp, M. E. Hegi, T. Gorlia, S. C. Erridge, J. Perry, Y.-K. Hong, K. D. Aldape, B. Lhermitte, T. Pietsch, D. Grujicic, J. P. Steinbach, W. Wick, R. Tarnawski, D.-H. Nam, P. Hau, A. Weyerbrock, M. J. B. Taphoorn, C.-C. Shen, N. Rao, L. Thurzo, U. Herrlinger, T. Gupta, R.-D. Kortmann, K. Adamska, C. Mcbain, A. A. Brandes, J. C. Tonn, O. Schnell, T. Wiegel, C.-Y. Kim, et al., *Lancet Oncol.* **2014**, *15*, 1100.
[106] C. Yang, M. Cao, H. Liu, Y. He, J. Xu, Y. Du, Y. Liu, W. Wang, L. Cui, J. Hu, F. Gao, *J. Biol. Chem.* **2012**, *287*, 43094.
[107] V. B. Lokeshwar, N. Fregien, L. Y. W. Bourguignon, *J. Cell Biol.* **1994**, *126*, 1099.
[108] M. Roszkowska, A. Skupien, T. Wójtowicz, A. Konopka, A. Gorlewicz, M. Kisiel, M. Bekisz, B. Ruszczycki, H. Dolezyczek, E. Rejmak, E. Knapska, J. W. Mozrzymas, J. Wlodarczyk, G. M. Wilczynski, J. Dzwonek, *Mol. Biol. Cell* **2016**, *27*, 4055.
[109] J. W. Legg, C. A. Lewis, M. Parsons, T. Ng, C. M. Isacke, *Nat. Cell Biol.* **2002**, *4*, 399.
[110] B. Amsden, *Macromolecules* **1998**, *31*, 8382.
[111] A. E. Rizzardi, A. T. Johnson, R. I. Vogel, S. E. Pambuccian, J. Henriksen, A. P. N. Skubitz, G. J. Metzger, S. C. Schmechel, *Diagn Pathol* **2012**, *7*, 42.
[112] S. Bastola, M. S. Pavlyukov, D. Yamashita, S. Ghosh, H. Cho, N. Kagaya, Z. Zhang, M. Minata, Y. Lee, H. Sadahiro, S. Yamaguchi, S. Komarova, E. Yang, J. Markert, L. Nabors, K. Bhat, J. Lee, Q. Chen, D. Crossman, K. Shin-Ya, D. Nam, I. Nakano, *Nat. Commun.* **2020**, *11*, 1.